Chapter 5 *Thickness Dependent Phase Transformation and Resistive Switching Performance of HfO_2 Thin Films Fabricated by Ion Beam Sputtering*

5.1 Introduction

Resistive random access memory (RRAM) devices are being investigated extensively for future nonvolatile memories using various transition metal oxides such as NiO, ZnO, TiO_2 and HfO_2 as the active material. In this chapter, we have demonstrated the performance of RRAM devices using HfO_2 thin films deposited by the ion beam sputtering technique on p^{++}-Si (100) substrate with varying thickness from 10 to 30 nm. The structure and microstructure analysis of the films is provided in section 5.2. A drastic change in the average grain size from ~ 90 to ~ 2000 nm is noticed along with a structural transformation from orthorhombic to dominant monoclinic phase when the thickness is increased from 20 to 30 nm. The bipolar forming-free resistive switching performance of the RRAM devices fabricated using these films is presented in section 5.3. Among all films, the film of 20 nm thickness shows better switching behavior with an ON/OFF ratio of ~ 7 attributed to the appropriate grain size, enhanced crystallization and oxygen vacancies. The endurance and retention measurements show the excellent reliability in case of the 20 nm thick film. Schematically, the switching mechanism has been discussed based on the Ohmic and Poole-Frenkel conduction models, which is attributed to the formation and rupture of conductive filaments consisting of oxygen vacancies. The results of this chapter are concluded in section 5.4.

5.2 Structure and Microstructure

5.2.1 Thickness, Density and Roughness by X-ray Reflectivity

Ion beam sputtered HfO_2 thin films of thickness 10, 20 and 30 nm are denoted as HO10, HO20 and HO30, respectively. X-ray reflectometry (XRR) spectra for HO10, HO20 and HO30 thin films are represented in **Figure 5.1**. To estimate the film thickness, density, and roughness, appropriate stack models are used to fit the XRR spectra with Parratt32 software. The insets of **Figure 5.1** show the schematic diagram of stacking models used for the fitting. The critical angle for external reflection determines density, while the period of the oscillations gives thickness. The fittings demonstrate that in all three films, the observed pattern and simulated curves match very well with each other. At the start of the film growth process, an interface layer of Hf-silicate with about 1.5 nm thickness is formed in the case of each film. The estimated thickness of HfO_2 film is found to be ~ 10, 18 and 26 nm; and density is 9.1, 8.9 and 8.6 g/cm^3 corresponding to HO10, HO20 and HO30, respectively. The surface roughness is calculated to be 0.4 nm for HO10, whereas 0.6 nm is obtained for both HO20 and HO30 films.

5.2.2 Surface Morphology by Atomic Force Microscopy

The surface morphology of the thin films is obtained from atomic force microscopy (AFM) and depicted in **Figure 5.2**. The insets of **Figure 5.2** show the enlarged view of micrographs and grain size histograms for HO10 and HO20. The average grain size of HO10 and HO20 is ~ 50 and ~ 90 nm, respectively, whereas it is ~ 2000 nm for HO30. The grain size of HO30 is found to be much larger than the grain size of HO10 and HO20. Hence, the higher the film thickness, the higher is the grain size.

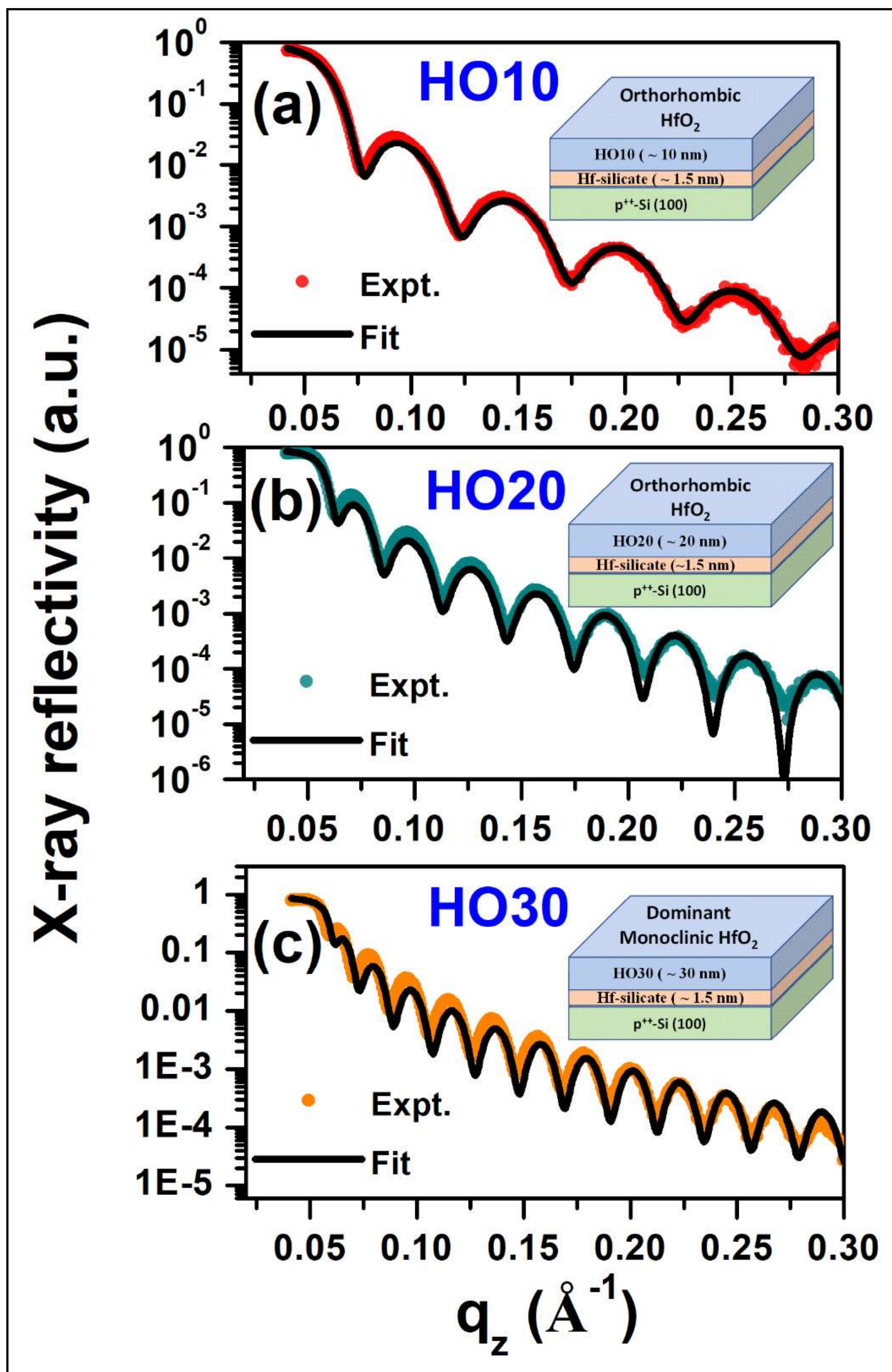

Figure 5.1 *X-ray reflectivity spectra of HfO_2 thin films having thicknesses of ~ 10, 20 and 30 nm. Insets show the schematic diagram of the stacking used for fitting the XRR spectra (diagrams are not to scale).*

Surface roughness calculated from the micrographs for HO10, HO20 and HO30 thin films is 0.3, 0.6 and 0.7 nm, respectively, which are very close to the roughness estimated from the XRR. The minimum surface roughness of the active layer plays a substantial role in minimizing the leakage current in the electronic devices and supports the local charge transport [150].

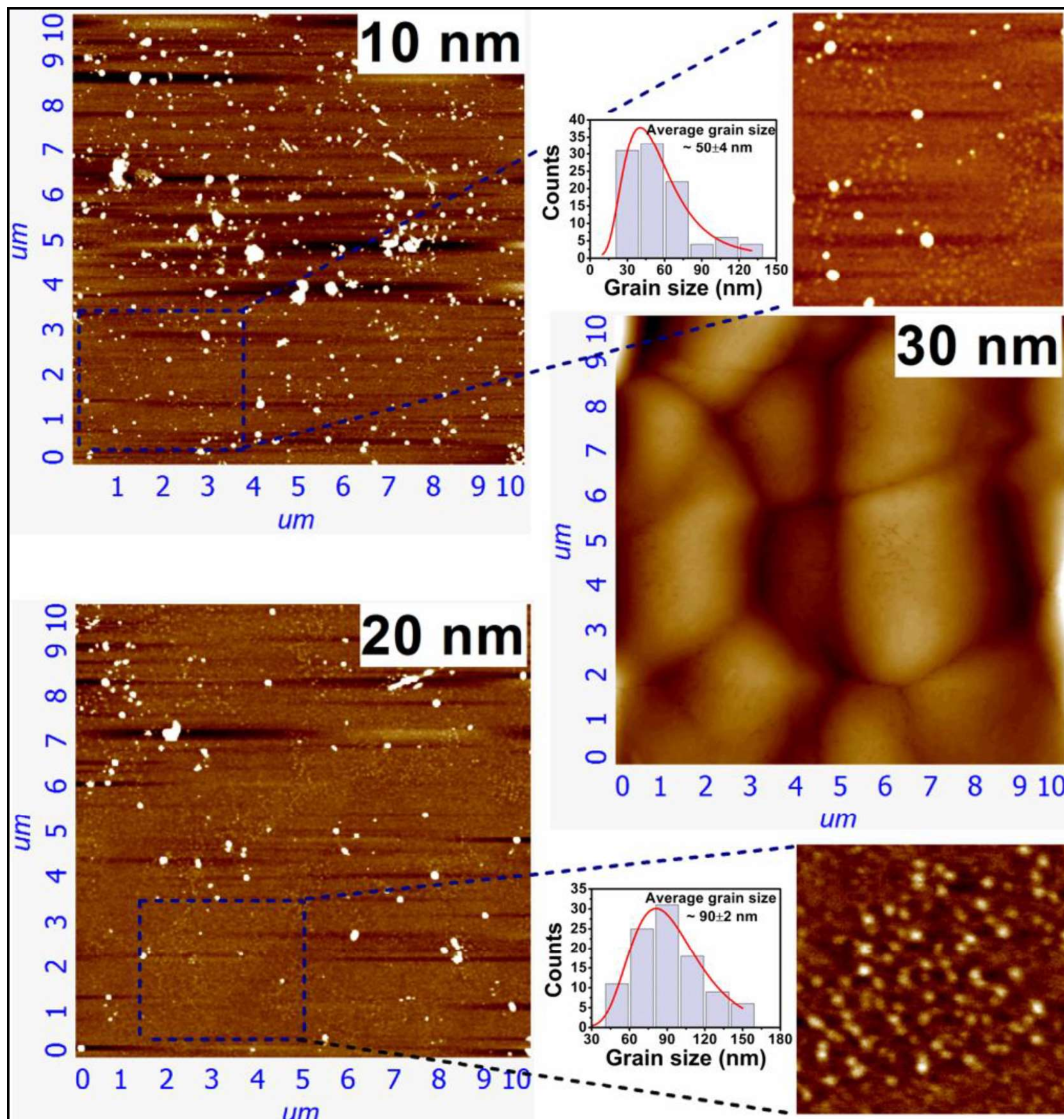

Figure 5.2 *AFM analysis of the fabricated HfO_2 thin films of ~ 10, 20 and 30 nm thickness. The film roughness is found to be 0.3, 0.6 and 0.6 nm for 10, 20 and 30 nm films, respectively.*

5.2.3 Structure and Phase Transformation

The grazing incidence X-ray diffraction (GIXRD) patterns of HO10, HO20 and HO30 depicted in **Figure 5.3** show the diffraction peak observed at ~ 44.2^0 corresponds to (141) of orthorhombic phase (space group: *Pbca*) of HfO_2 in the case of HO10 film. Along with the above peak, an additional peak at ~ 30.6^0 corresponding to (121) has been detected in HO20, which belongs to the same orthorhombic phase. The absence of any extra peak confirms that both HO10 and HO20 exhibit pure orthorhombic phase. For HO30, the diffraction peaks at $2\theta \sim 28.3^0$, 35.5^0, 51.1^0, 55.7^0 and 60.8^0 are identified as (-111), (200), (-221), (221) and (-302), respectively, of monoclinic phase (space group: *P21/c*) of HfO_2. In addition, an extra peak at 30.6^0 corresponding to (121) of the orthorhombic phase, *Pbca* space group, is detected. Here, both HO10 and HO20 are single crystalline films with a preferred growth direction of (141) of orthorhombic phase, whereas HO30 exhibits polycrystallinity. One may notice that with the increase in the film thickness from 10 to 30 nm, the structural phase transformation from pure orthorhombic phase to a mixed phase of monoclinic and orthorhombic has been detected. The thickness dependent phase transformation could be induced due to the increase in the grain size as observed from the AFM micrographs (**Figure 5.2**). Such thickness dependent phase transformation in HfO_2 has not been investigated earlier to the best of our knowledge. Earlier, we have shown the monoclinic to cubic phase transformation in the rare-earth (Dy, Sm, Pr) doped HfO_2 nanoparticles where oxygen vacancies play a crucial role [29,30,147]. Additionally, we report the monoclinic to cubic phase transformation in rare-earth (Dy, Sm) doped HfO_2 thin films, which is also attributed to the enhancement of oxygen vacancies by the introduction of rare-earth ions in the HfO_2 matrix [105]

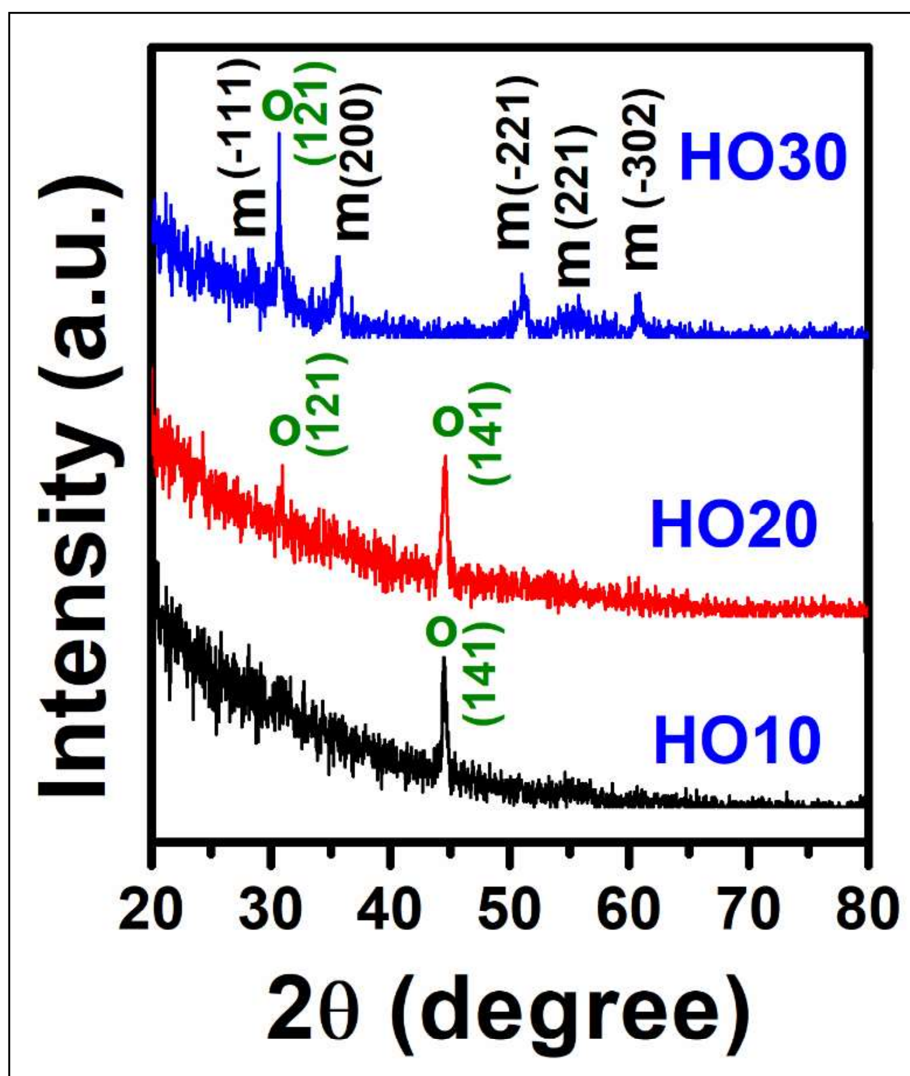

Figure 5.3 *GIXRD data for HfO_2 thin films with ~ 10, 20 and 30 nm thickness [m = monoclinic (P21/c), o = orthorhombic (Pbca) phase].*

5.2.4 X-ray Photoelectron Spectroscopy and UV-visible Spectroscopy

Therefore, to study the role of oxygen vacancies in the present case, we carry out the X-ray photoelectron spectroscopy (XPS) analysis of HO20 and HO30 films. All the spectra are corrected with respect to the carbon 1*s* peak positioned at 284.6 eV and are analyzed using XPSPEAK41 software. **Figure 5.4 (a)** and **(b)** show the XPS spectra of Hf 4*f* core

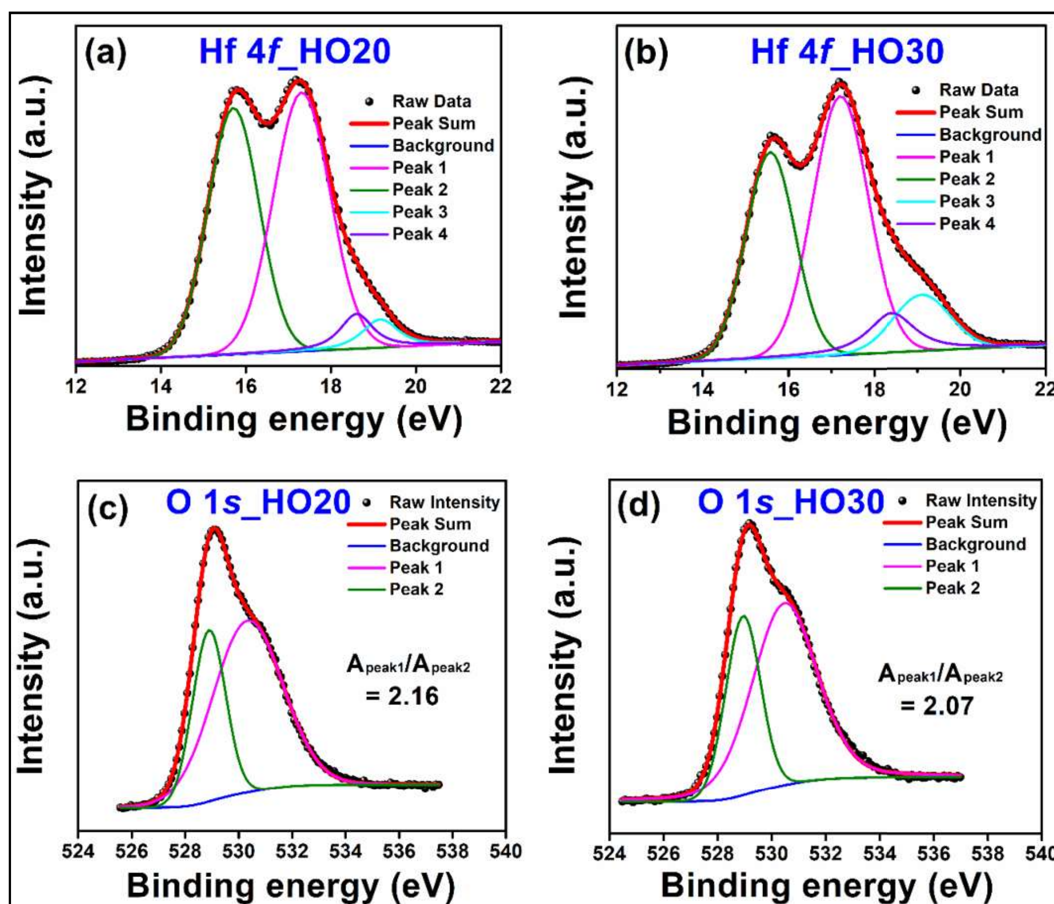

Figure 5.4 *(a, b) Hf 4f and (c, d) O 1s core level XPS spectra of oxygen deficient HfO_2 thin films having thicknesses of ~ 20 and 30 nm.*

level HO20 and HO30 films. We have deconvoluted the Hf 4*f* spectra into four different peaks. The two peaks located at 15.7 and 17.3 eV corresponding to Hf $4f_{7/2}$ and Hf $4f_{5/2}$, respectively, represent the oxygen deficient hafnium oxide films [151,152]. The other two peaks at 18.6 and 19.1 eV are attributed to the Hf 4*f* peaks of the stoichiometric hafnium oxide film [151]. The enhancement in the area of peaks at 18.6 and 19.1 eV with the increase in the thickness of the film from 20 to 30 nm indicates the reduction of oxygen vacancies, which can be further confirmed from the O 1*s* spectra demonstrated in **Figure 5.4 (c)** and **(d)**. Due to the asymmetric shape, the O 1*s* spectra are deconvoluted into two different peaks, namely peak 1 and peak 2, which are centered around 530.5 and 529 eV, respectively. The peak at 530.5 eV is ascribed to oxygen deficient regions

exhibiting oxygen vacancies and oxygen ions in Si-O bonds, whereas the peak at 529 eV is attributed to lattice oxygen atoms in Hf-O bonds [29,147,153]. The ratio of area under peak 1 and peak 2, i.e., (A_{peak1}/A_{peak2}), is found to be 2.16 and 2.07 in HO20 and HO30 films, respectively. The oxygen vacancies are generally created at the grain boundaries. As the thickness of the film increases, the average grain size increases, causing a decrease in the grain boundary area. Therefore, the oxygen vacancy concentration in the film decreases with the increase in film thickness [154]. Even though the oxygen vacancy in the HO20 film is higher than that of the HO30 film, it may not be significant in showing a phase transformation from orthorhombic to monoclinic. However, the average grain size is almost an order of magnitude higher in the monoclinic phase than that in the orthorhombic phase. Hence, in the present case, not only the oxygen vacancy but also the average grain size plays a key role in the phase transformation from orthorhombic to monoclinic phase by increasing thickness from 20 to 30 nm.

Further, the role of grain size has been examined from the absorption spectra obtained by UV-visible spectroscopy. The absorption spectra of HO20 and HO30 films depicted in **Figure 5.5 (a)** show the absorption peaks at 248 and 312 nm, respectively. With the increase in thickness, the absorption peak shows a redshift. The direct optical band gap (E_g) of these films is calculated using the Tauc equation given below:

$$(\alpha h\nu) \propto \left(h\nu - E_g\right)^{1/2} \tag{5.1}$$

where α and $h\nu$ are the absorption coefficient and the photon energy, respectively, depicted in **Figure 5.5 (b)** [155,156]. The band gap decreases drastically from 4.5 eV in HO20 to 3.7 eV in HO30. The decrease in the band gap confirms the increase in the grain size, which creates several intermediate energy levels within the band gap region as a result of the symmetry breach [157]. In contrast to our earlier reports on rare-earth doped HfO_2 nanoparticles and thin films where oxygen vacancies play a crucial role in the phase

transformation from low symmetry monoclinic phase to high symmetry cubic phase, in the pristine HfO_2 films of different thickness average grain size plays a significant role in the phase transformation.

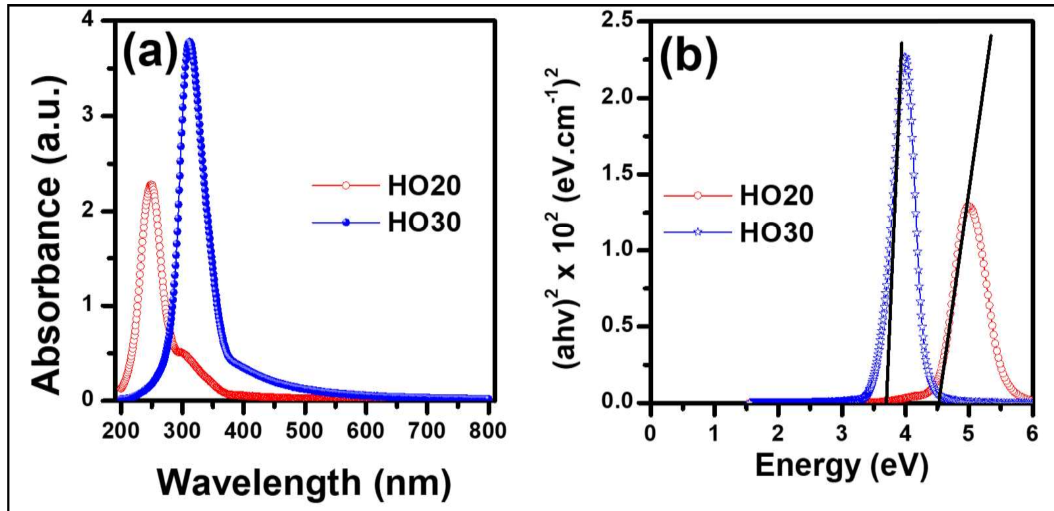

Figure 5.5 *(a) Absorbance spectra and (b) band gap of HfO_2 thin films with thicknesses of ~ 20 and 30 nm.*

5.3 Resistive Switching Behavior

5.3.1 Current-Voltage (*I-V*) Characteristics

The role of oxygen vacancy has been examined for the performance of RRAM devices in these films. The resistive switching behavior of HfO_2 films is examined from *I-V* characteristic curves, which are depicted in **Figure 5.6**. We have shown the 1st, 50th, and 100th *I-V* cycles for each HfO_2 film. After sweeping the applied DC bias voltage in a cycle of 0 V → -3 V → 0 V → 3 V → 0 V, *I–V* measurements are carried out. The bias voltage is applied to the top electrode while the bottom electrode is grounded throughout the measurement. The compliance current during switching measurement has been set at 7 mA to prevent the electrical breakdown of the device. A very small current at the first

stage (0 to -3 V) indicates the HRS or OFF state. The current displays an abrupt increase, suggesting a switch to the LRS or ON state at a specific bias voltage known as SET voltage (V_{SET}). Likewise, in the positive bias voltage range (0 to 3 V), the bias voltage at which the current abruptly drops is identified as the RESET voltage (V_{RESET}). The presence of negative V_{SET} and positive V_{RESET} confirms the characteristic bipolar resistive switching behavior of the HfO_2 based RRAM devices. Remarkably, in this case, the resistive switching behavior is forming-free in nature with no capping layer. Nevertheless, Hua *et al.* show that a HfO_2 based RRAM device exhibits the forming-free resistive switching behavior with a thin capping layer of Ti [103]. We have used the *I-V* data of the 100th cycle to calculate the value of V_{SET}. HO10 and HO20 having orthorhombic phase exhibit a V_{SET} value of -2.64 V, whereas V_{SET} is estimated to be -2.33 V in the case of HO30 film having a dominant monoclinic phase. Similar values of V_{SET} of RRAM devices based on HfO_2 thin films doped with Al and Cu are reported by Ning *et al.* [158]. Also, the ON/OFF ratio is estimated to be ~ 2 and 7 at a readout voltage of 1 V for HO10 and HO20, respectively, which is nearly close to the ON/OFF ratio calculated for monoclinic (~ 3), cubic (~ 3) and tetragonal phase (~ 5) HfO_2 based RRAM devices in the earlier reports [105,159]. The increase in the ON/OFF ratio in HO20 than that of HO10 is attributed to the enhanced crystallization of the orthorhombic phase in HO20, as observed from the XRD [160]. **Figure 5.7** represents the SET and REST voltage distribution of five different devices based on 20 nm thick of HfO_2 film. The SET and RESET voltages remain almost constant across all five devices confirming no device-to-device variation.

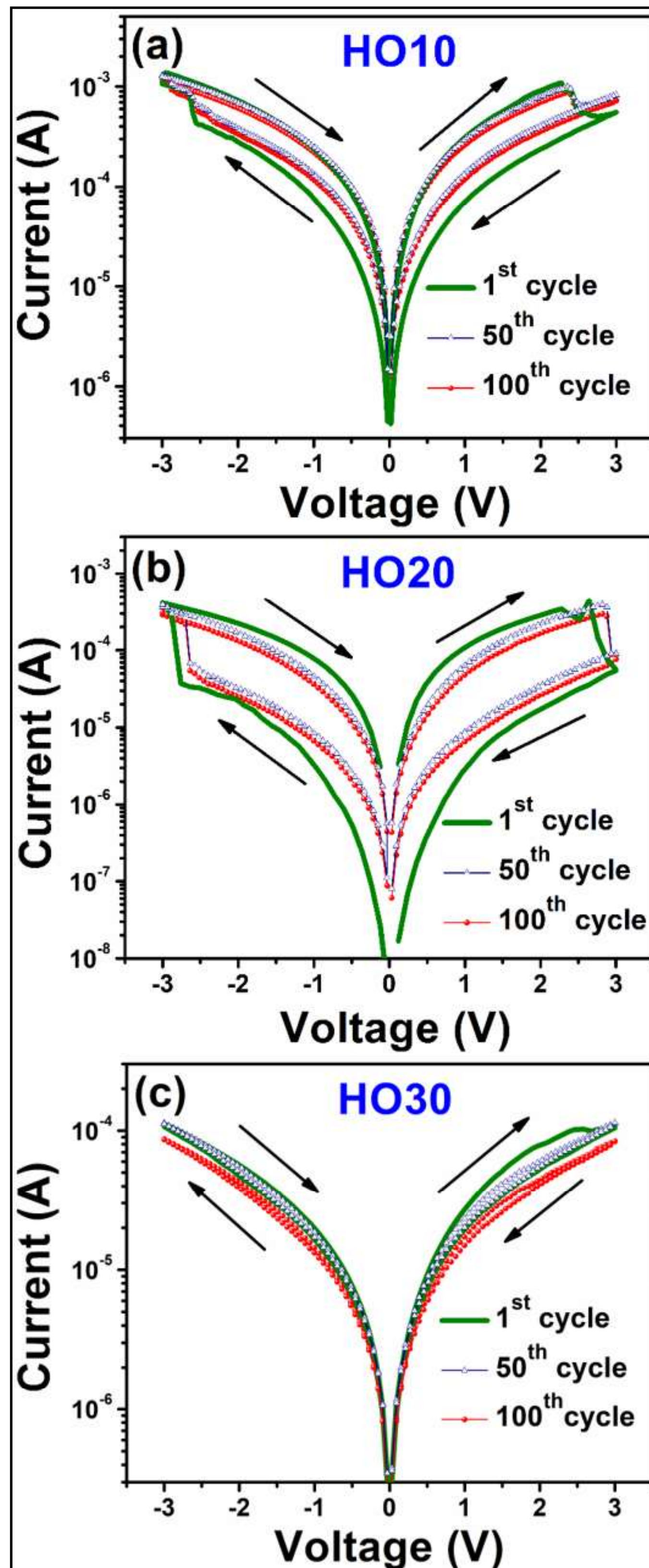

Figure 5.6 *Current-voltage (I-V) characteristics in semilogarithmic scale for RRAM devices based on HfO_2 films of ~ 10, 20 and 30 nm thickness.*

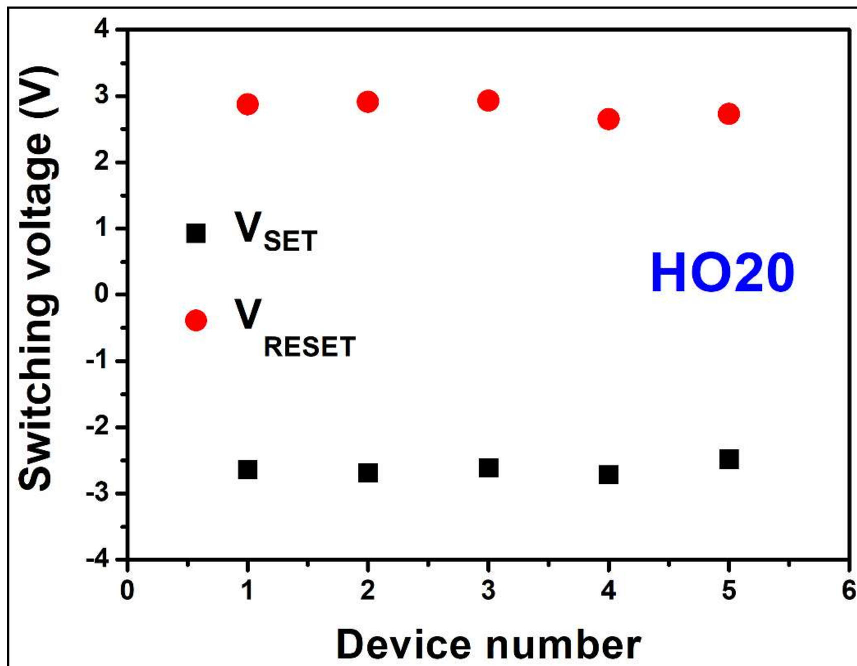

Figure 5.7 *SET and RESET voltage distribution of five RRAM devices based on HfO_2 film of 20 nm thickness.*

The ON/OFF ratio of HO30 decreases drastically, which is ~ 1 at a readout voltage of 1 V. We have increased the applied voltage up to -7 V to examine the *I-V* characteristics of the RRAM device based on HO30. But, still, the current does not reach the compliance current limit, and there is no improvement in the ON/OFF ratio (**Figure 5.8**). The higher ON/OFF ratio of HO20 could be due to the more oxygen vacancy present in the orthorhombic phase. The decrease in the separation between ON and OFF states in mixed phase HO30 is because of the leakage current due to the increase in the grain size with large grain boundaries and the decrease in the oxygen vacancies, as confirmed by AFM and XPS measurements.

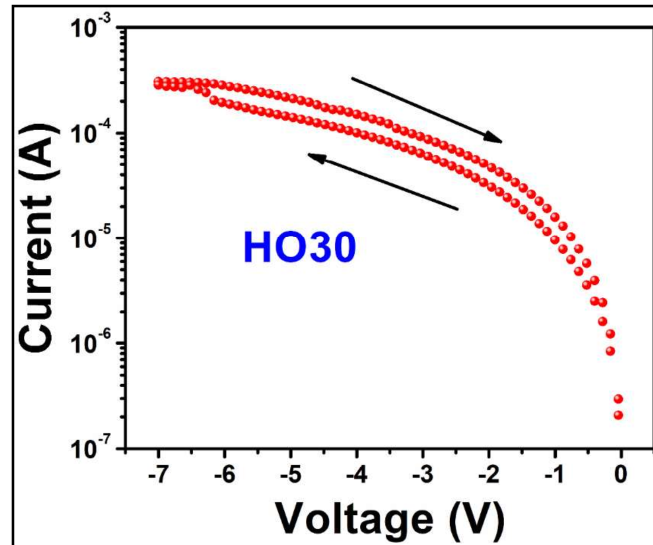

Figure 5.8 *Current-voltage (I-V) characteristics in semilogarithmic scale for RRAM devices based on HfO_2 film of 30 nm thickness.*

5.3.2 Endurance and Retention Measurements

In order to investigate the stability and reliability of the devices, the endurance and retention properties are presented in **Figure 5.9**. The endurance characteristics of the devices are examined at a readout voltage of 1 V and shown in **Figure 5.9 (a)**. The R_{LRS} and R_{HRS} of the HO20 film show no significant failure after 100 consecutive RS cycles. The retention stability of the HfO_2 films is measured at a readout voltage of 1 V, as presented in **Figure 5.9 (b)**. The current of RRAM based on HO20 is stable with a relatively higher storage window than HO10 and HO30, and can maintain up to 10^4 s without any noticeable degradation.

5.3.3 Mechanism for Resistive Switching

We study various conduction models, including Ohmic conduction, Fowler–Nordheim (F–N) tunneling, Schottky emission, Poole–Frenkel (P–F) emission, and space charge

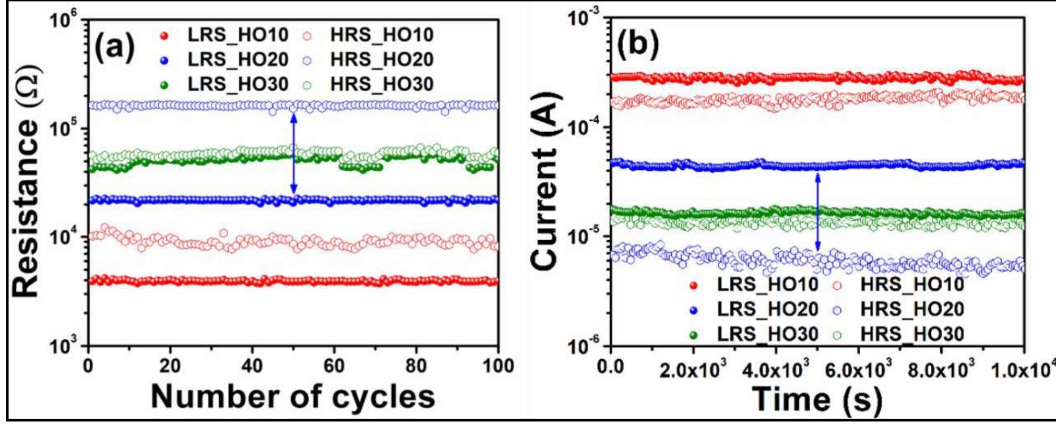

Figure 5.9 *(a) The endurance and (b) the retention characteristics at a readout voltage of 1 V of RRAM devices based on HO10, HO20, and HO30. The double-sided arrow indicates the storage window of the RRAM device based on HO20.*

limited current (SCLC) in LRS and HRS states to develop a thorough understanding of SET and RESET mechanisms [95]. The relationships between current and voltage as per the Ohmic conduction and Poole–Frenkel emission models are defined as the following equations:

$$I \propto Ve^{\frac{-A}{T}} \quad \textbf{(5.2)}$$

and

$$I \propto Ve^{\frac{q\,(2a\sqrt{V}-\phi_B\,)}{kT}} \quad \textbf{(5.3)}$$

where A is a constant, T is the temperature, $a = \sqrt{\frac{q}{4\pi\varepsilon_i d}}$, ε_i is the electric field in the dielectric, d is the thickness of the dielectric, ϕ_B is the barrier height, and k is the Boltzmann constant [161]. The fitting of *I-V* characteristics of HO20 in the log-log scale is shown in **Figure 5.10 (a)**, which confirms the linear relationship with a slope of 1.7. The graph demonstrates that the Ohmic conduction model dominates in the entire LRS state. Also, the conduction behavior in the low voltage region for the HRS state adheres

to the Ohmic model. When the carrier density generated by thermal effects is significantly more than the intrinsic carrier density, Ohmic conduction prevails. However, the conduction mechanism is not the same and does not behave linearly in the high voltage regime of HRS. Applying a nonlinear conduction mechanism, such as Poole–Frenkel emission, allows us to perceive this behavior. **Figure 5.10 (b)** displays the linear fitting of *I-V* characteristic curves by the Poole–Frenkel emission model in the high applied bias voltage regime of the HRS state in HO20. It is validated that the primary conduction mechanism in the high electric field region is Poole–Frenkel emission. The leading cause of Poole–Frenkel emission conduction in HfO_2 films is crystallographic defects such as single (V_o^+) or doubly (V_o^{++}) charged oxygen vacancies [105,162].

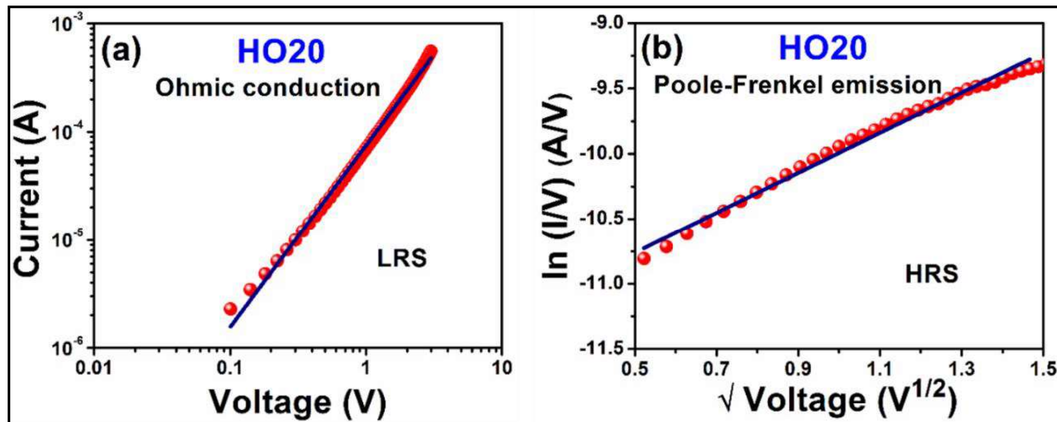

Figure 5.10 *(a) Ohmic and (b) Poole-Frenkel model linear fits for LRS and HRS, respectively, for 20 nm HfO_2 film (Ohmic model is shown in log-log scale).*

Moreover, the formation (creation) of conductive filaments (CFs) through migration of oxygen vacancies/oxygen ions, Schottky barrier, and trapped charged carriers has mostly been used to explain the resistive switching behavior [163]. Among them, there is a lot of research being done on the localized creation and destruction of CFs inside the dielectric active layer. It is well established that localized nanosized CFs are formed in

oxide films at low bias voltages, which agglomerate to form stronger and more conductive CFs at higher applied bias voltages. Zhang *et al.* explore that RRAM behavior increases through Gd doping in the HfO_2 lattice by diminishing the randomized characteristic of CFs, thus minimizing the barrier of oxygen ion migration [164]. The report by Lee *et al.* reveals that Gd and Dy doped ZrO_2 devices display switching behavior because of the adequately large concentration of oxygen vacancies induced by the dopants, while Ce doped ZrO_2 based RRAM demonstrates the preliminary formation of CF, which is attributed to enhanced crystallization [160]. To verify the experimental evidence, a theoretical model has been proposed by Rozenberg *et al.* that accounts for the bipolar resistive switching phenomenon observed in transition metal oxides [165]. This model assumes three key features: (a) electric transport dominated by a single conductive path embedded within a more insulating host, (b) relevance of the significant number of oxygen vacancy (V_o) defects within the dielectric, and (c) role of interface between the dielectric and the metallic electrode, to correctly reproduce the hysteresis cycles. It qualitatively describes the electric field enhanced migration of oxygen vacancies at the nanoscale. *P-V* loops of HfO_2 thin film of 20 nm thickness (HO20) show lossy behavior due to the non-uniform orientation of the dipoles inside the HO20 film at a higher external voltage (**Figure 5.11**). The polarization value at the SET voltage (-2.64 V) for HO20 based RRAM is very small compared to the polarization values at the voltages of lower magnitude. Although Schottky barrier modulation at the interface of the HfO_2 layer and electrode as the manifestation of induced polarization can affect the resistive switching behavior [166], the small polarization due to the lossy behavior of the film eliminates its contribution towards the resistive switching. Therefore, the presence of an appropriately high concentration of V_os, along with enhanced crystallization in HO20, predominantly contributes to better resistive switching behavior.

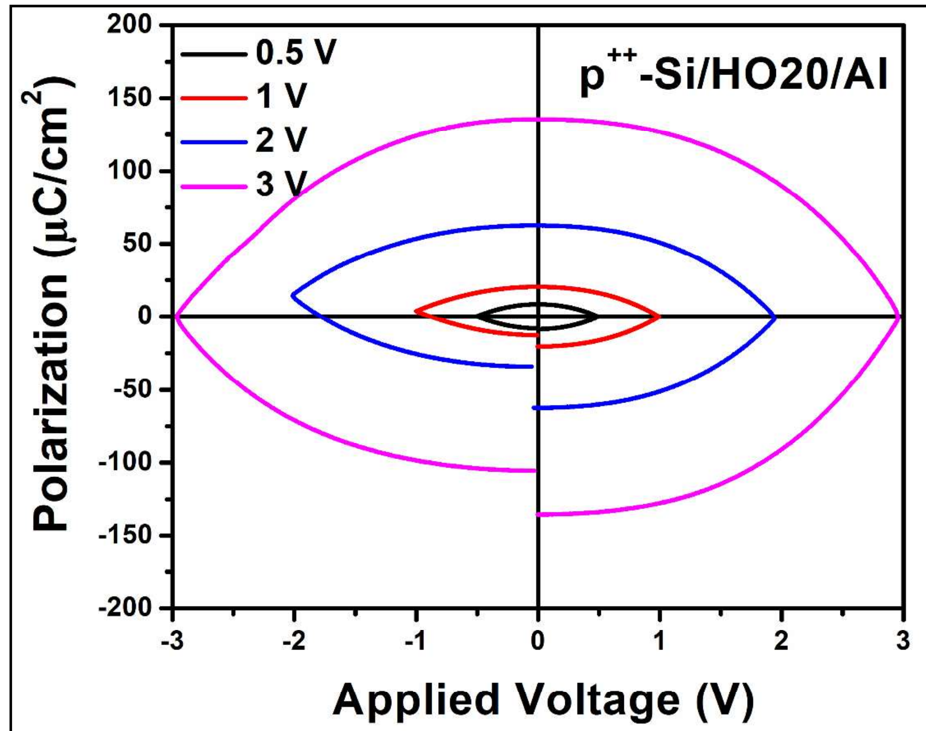

Figure 5.11 *P-V loops obtained from hysteresis measurements of HfO_2 thin film of 20 nm thickness (HO20).*

In **Figure 5.12**, a schematic demonstration of the proposed mechanism is provided for resistive switching through the formation of CFs in HfO_2 based RRAM devices. At zero bias voltage, the memory device is at the HRS state where V_os are randomly oriented in the HfO_2 film, as represented in **Figure 5.12 (a)**. These positively charged V_os move towards the top electrode (TE) and accumulate there when a negative bias is applied to the TE. The accumulating V_os transform into the nuclei of CFs since V_os may produce an acceptor level close to the valence band, which is the origin of hole-electron carriers. These nuclei subsequently expand towards the bottom electrode (BE) and act as extensions of the TE. The memory device switches into the LRS state once a complete CF has formed, as depicted in **Figure 5.12 (b)**. When the TE is positively biased, the majority of the Joule heat is produced at the TE end of the CF, thereby substantially fast-tracking the mobility of V_os in this area. V_os in this area move fast towards the BE under

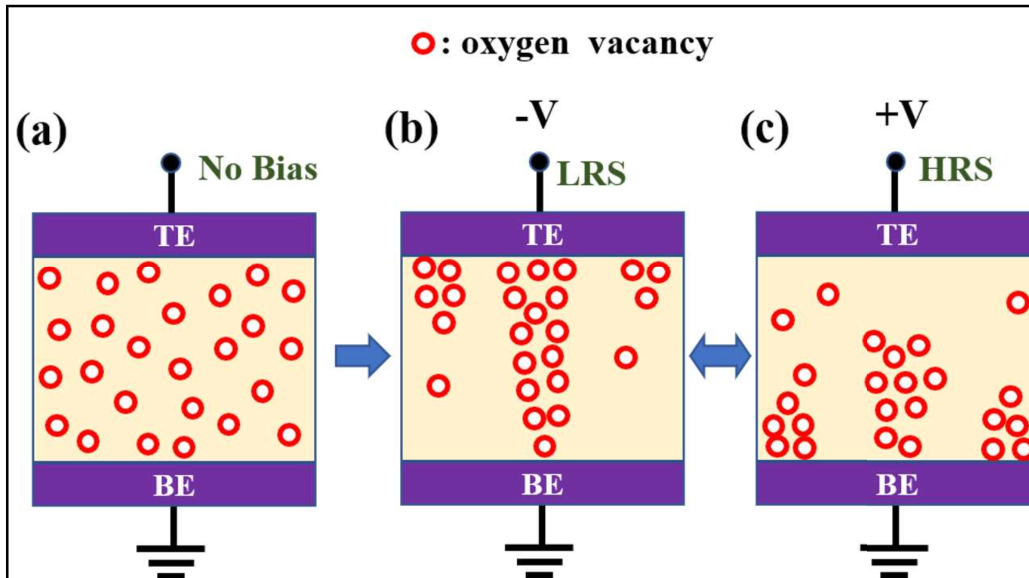

Figure 5.12 *Resistive switching mechanism in oxygen deficient of HfO_2 thin films (TE- top electrode, BE- bottom electrode, LRS- low resistance state, HRS- high resistance state).*

the influence of the electric field and are annihilated by the oxygen ions present at the active layer/BE interface or at the grain boundaries of the BE. Consequently, the concentration of V_os in the TE end of the CF is reduced considerably, leading to the rupture (destruction) of the CF at that site, resulting in the switching of the memory cell to the HRS state (**Figure 5.12 (c)**). Thus, it is concluded that HO20 based RRAM device shows well-regulated resistive switching behavior due to the small grain size, enhanced crystallization of the orthorhombic phase, and abundance of oxygen vacancies. This device may be utilized for next-generation data storage as well as in neuromorphic computing devices.

5.4 Conclusions

In this work, we deposited HfO_2 films using the ion beam sputtering technique on highly doped p-type Si (100) substrates with various thicknesses. While the thickness of the film

estimated from the XRR was found to be around 10, 20, and 30 nm, the density was estimated to be in the range of 9.1-8.6 g/cm^3. The average grain size of the films calculated from the AFM showed a radical enhancement of the grain size from ~ 90 nm in the film of thickness 20 nm to ~ 2000 nm in the film of thickness 30 nm. XRD patterns confirmed an orthorhombic phase in films of thickness 10 and 20 nm, and a dominant monoclinic phase in film of thickness 30 nm. Such phase transformation was accompanied by the enormous increase in grain size along with the reduction in oxygen vacancies observed from XPS. The forming-free resistive switching behavior of these films was investigated from 100 *I-V* cycles. The film of 20 nm thickness exhibited better switching characteristics than that of the 30 nm film. HfO_2 film of 20 nm thickness displayed a separation of ~ 7 between ON and OFF states. The reliability and stability of the RRAM device based on 20 nm thick HfO_2 film are confirmed from the endurance (for 100 cycles) and retention (up to 10^4 s) measurements. We fitted the *I-V* data with suitable conduction models and found that Ohmic conduction dominated the LRS, whereas Poole-Frenkel conduction dominated the HRS. The resistive switching behavior was attributed to the formation and rupture of conductive filaments involving oxygen vacancies by applying negative and positive bias in the film of 20 nm thickness.